A Common Mode Inductor With External Magnetic Field Immunity, Low-Magnetic Field Emission, and High-Differential Mode Inductance

Yongbin Chu, *Student Member, IEEE*, Shuo Wang, *Senior Member, IEEE*, Ning Zhang, and Dianbo Fu, *Member, IEEE*

Abstract—This paper proposes a stacked common-mode (CM) inductor for electromagnetic interference (EMI) attenuation. The proposed stacked CM inductor consists of two CM inductors with identical cores and the same number of winding turns but with opposite winding directions. The proposed stacked CM inductor has three advantages. First, it is much less susceptible to external magnetic field interference than conventional CM inductors. This suppresses the EMI due to the near-magnetic-field coupling to the CM inductor. Second, the proposed winding structure effectively increases the leakage inductance of the CM inductor, which enhances its ability to suppress differential-mode (DM) noise. Third, the magnetic field generated by the DM current in the stacked CM inductor is partially canceled outside of the inductor. As a result, the stacked CM inductor has lower magnetic field emission than that of a conventional CM inductor. Simulation and experimental results validate the advantages of the proposed CM inductor, which show the proposed technique greatly improves the performance of CM inductors.

Index Terms—Common-mode (CM) inductor, leakage inductance, magnetic field, near-magnetic-field coupling, stacked inductor.

I. INTRODUCTION

POWER electronics research has continuously focused on high power density and high switching frequency solutions in the last decade. However, a high switching frequency may lead to severe electromagnetic interference (EMI) issues [1]–[4]. At the same time, a compact design inevitably decreases the distances between the EMI filters and the main power circuits in power electronics systems. Therefore, the EMI filters will easily pick up near-magnetic-field noise emitted from the main power circuits. This significantly degrades the performance of the EMI filters. Because of this, the EMI filters are usually overdesigned [1], [2]. In fact, EMI filters may take up to 50% of the total volume and weight and be one of the largest functional units
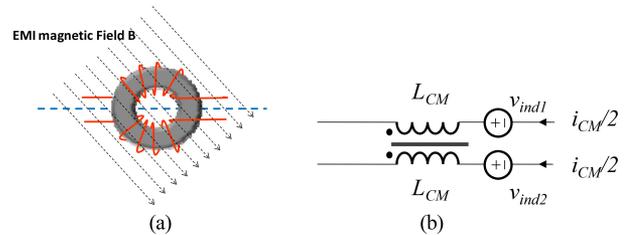
Fig. 1. Generation of noise voltages in a CM inductor due to near-magnetic-field coupling: (a) CM inductor in a magnetic field and (b) its equivalent circuit.

in power electronics systems. The reduction of the size of EMI filters plays an important role in the development of high power density converters.

A considerable amount of research has been conducted to improve the performance of EMI filters and reduce their size [1]–[21]. The near-magnetic-field coupling within an EMI filter has been modeled in [6]–[8] and techniques to reduce its effect on the performance of the EMI filter have been developed [1], [9]–[14]. The near-magnetic-field coupling between an EMI filter and a main circuit is also very important. For example, a CM inductor can become a noise source due to near-magnetic-field couplings. Although several articles [15]–[19] have discussed this issue, none of them have proposed an effective solution to it.

Fig. 1(a) shows a common-mode (CM) inductor in the presence of a time-varying magnetic field. The time-varying magnetic field generates a flux linkage within the inductor windings. This results in noise voltages in the windings as shown in Fig. 1(b). In Fig. 1(b), V_{ind1} and V_{ind2} are the induced voltages in the two windings. If the magnetic field is uneven or the CM inductor windings are asymmetric, the induced voltages V_{ind1} and V_{ind2} will be unequal. As a result, the near-magnetic-field coupling generates both CM and differential-mode (DM) noise. The induced CM noise voltage, V_{CM}, and DM noise voltage, V_{DM}, due to near-magnetic-field coupling are given by

$$V_{\text{CM}} = \frac{V_{\text{ind1}} + V_{\text{ind2}}}{2} \tag{1}$$

$$V_{\text{DM}} = \frac{V_{\text{ind1}} - V_{\text{ind2}}}{2}. \tag{2}$$

Additionally, when DM currents flow through the CM inductor, the CM inductor generates a leakage (DM) magnetic field. The generated magnetic field can be picked up by other components and traces in the circuit. Furthermore, the leakage
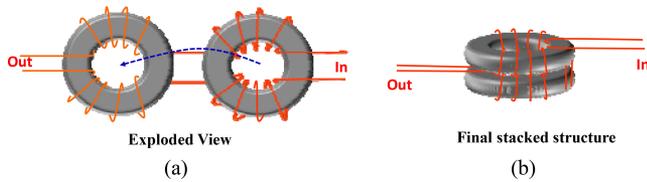
Fig. 2. Process to construct the proposed CM inductor: (a) exploded structure and (b) final stacked CM inductor.

Fig. 3. Equivalent circuit of a stacked CM inductor in an even external magnetic field.

inductance of CM inductors is usually used as DM inductance to attenuate DM noise and several techniques have been developed to increase the leakage inductance of CM inductors [3]–[5].

In this paper, a stacked CM inductor is proposed. It consists of two CM inductors with identical cores and the same number of winding turns but with opposite winding directions. The two CM inductors are connected in series and stacked. With this winding structure, the proposed CM inductor has three advantages over conventional CM inductors: 1) the proposed CM inductor is much less susceptible to an external near-magnetic-field than conventional CM inductors; 2) the proposed CM inductor has a larger DM inductance than conventional CM inductors; and 3) the proposed CM inductor has a lower magnetic field emission than conventional CM inductors.

In Section II, the working principle of the proposed stacked CM inductor is analyzed and a quasi-static magnetic solver (Ansys Maxwell 3-D) simulation is conducted to validate the analysis. Then, the experimental and measurement results in Section III verify the three advantages claimed aforesaid.

II. WORKING PRINCIPLE OF THE PROPOSED STACKED CM INDUCTORS

A. Principle of Voltage Cancellation

Fig. 2 shows the process to construct the proposed stacked CM inductor. First, two connected CM inductors with identical cores and the same number of winding turns but with opposite winding directions are assembled as shown in Fig. 2(a). Second, one CM inductor is stacked over the other in the manner indicated by the dashed arrow in Fig. 2(a). Fig. 2(b) shows the final stacked CM inductor. Since the two stacked CM inductors have identical cores and the same number of winding turns, their CM inductance should be the same. Furthermore, when the two CM inductors are stacked together, their original CM noise attenuation function will not be affected. Each CM inductor should be designed to have half of the desired CM inductance of the conventional CM inductor.

In Fig. 2(b), the two corresponding windings on each side of the two inductors are very close. As a result, when they are exposed to an even external magnetic field, the magnetic flux linkage of the two windings due to the external magnetic field will be similar. As a result, the induced noise voltages in the two corresponding windings on each side of the two inductors have similar amplitudes but opposite polarities. Because the two induced voltages are electrically in series, they are canceled as shown in Fig. 3. In Fig. 3, v_{ind1}, v_{ind2} and $-v_{\mathrm{ind1}}$, $-v_{\mathrm{ind2}}$ are the induced noise voltages within the windings of the two CM

inductors. Based on (1) and (2), both the induced CM and DM noise voltages are canceled out. Under practical conditions, the even external magnetic field could be from a different direction but the conclusion still holds.

It should be pointed out that the cancellation will be affected by the size of the CM inductor within an uneven external magnetic field. The reason is that as the size of the CM inductor increases, the difference between the magnetic flux linkages of the two corresponding windings on each side of the two inductors increases. This means the noise voltages induced in the two corresponding windings will be less completely canceled. As a result, a bigger proposed stacked CM inductor will become more susceptible to external magnetic field than a smaller one.

For the conventional CM inductor, if the number of turns is N, the mean length of the core is l, the cross-sectional area of the core is A, and the permeability of the core is μ, then the inductance, $L_{\mathrm{conventional}}$, and the volume, $V_{\mathrm{conventional}}$, of the conventional CM inductor (ignoring the volume of wires) can be expressed as

$$L_{\mathrm{conventional}} = \frac{\mu A}{l} N^2 \qquad (3)$$

$$V_{\mathrm{conventional}} = lA. \qquad (4)$$

For a fair comparison, the CM inductance and volume of the proposed stacked inductor in Fig. 2 should be the same as those of the conventional inductor in Fig. 1. The height of the cores of the proposed stacked inductor is half of that of the conventional CM inductor while the other dimensions are unchanged. The cross-sectional area of each core is therefore $A/2$. The number of turns and the permeability of the core are the same as those of the conventional inductor. The inductance and the total volume of the stacked CM inductor are, therefore, the same as those of the conventional CM inductor.

B. Increased DM Inductance

In addition to magnetic field immunity, the proposed stacked CM inductor has a bigger DM inductance than the conventional CM inductor. The leakage inductance of a CM inductor is usually used as DM inductance to filter out DM noise. Fig. 4(a) illustrates the magnetic flux distribution of a conventional CM inductor with a DM current excitation within its two windings.

For a CM inductor with a DM current excitation, the DM (leakage) magnetic flux is defined as the magnetic flux generated by one winding but not coupled to the other. In Fig. 4, B_1 and B_9 represent the DM magnetic flux from right to the left via the space above and below the inductor. $B_0, B_4,$ and B_8 represent the DM magnetic flux along the windings on the top and bottom
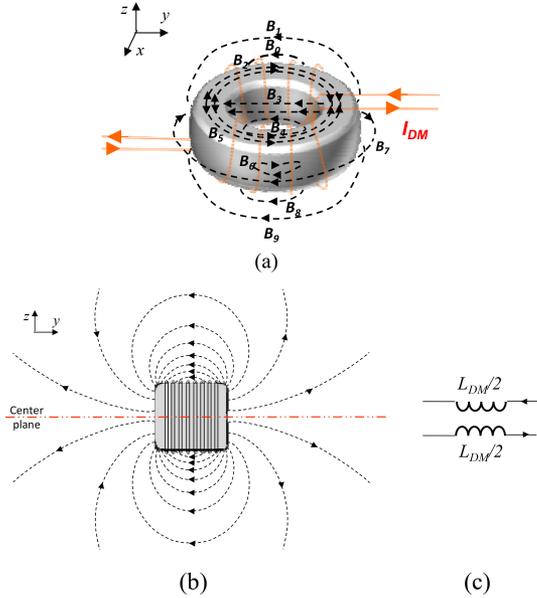
Fig. 4.   DM magnetic flux distribution of a CM inductor: (a) magnetic flux distribution, (b) side view, and (c) equivalent DM inductance L_{DM}.
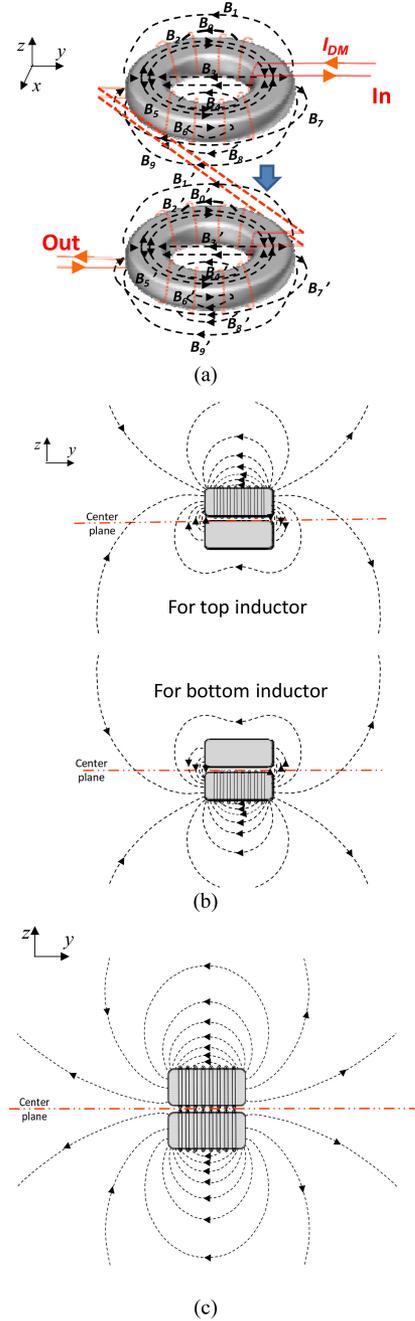

Fig. 5.   DM magnetic flux distribution of a stacked inductor with same winding direction is similar to that of a conventional inductor: (a) two inductors that stacked together with the same winding directions, (b) DM magnetic flux distribution of the two inductors, and (c) side view of the DM magnetic flux distribution of the stacked inductor (the magnetic flux in front of the inductor is not shown).

of the inductor. B_2 and B_5 represent the DM magnetic flux within the core. B_3 represents the DM magnetic flux within the inner surface of the core. B_6 represents the DM magnetic flux along the windings on the sides of the inductor (only the magnetic flux on the front side is shown in the figure). B_7 represents the DM magnetic flux from the right side to the left side via the space in front of the inductor (only the magnetic flux on the front side is shown in the figure). Fig. 4(b) shows the side view of the magnetic flux distribution. Only the magnetic flux outside the inductor is illustrated. The magnetic flux distribution is symmetric about the center plane and parallel to it on the plane. The equivalent circuit is shown in Fig. 4(c) and the equivalent DM inductance L_{DM} is given by (5), where L_W is the self-inductance of each winding and M_W is the mutual inductance of the two windings

$$L_{\mathrm{DM}} = 2L_W - 2M_W. \tag{5}$$

To better demonstrate the advantages of the proposed stacked CM inductor, two cases will be analyzed and compared. In the first case, a stacked CM inductor composed of two inductors with identical cores, the same number of turns and in the same winding direction will be analyzed. In the second case, the proposed stacked inductor will be analyzed.

Fig. 5(a) shows the exploded view of the stacked inductor in the first case. Each individual inductor has a DM magnetic flux distribution similar to Fig. 4(a) before stacking. After the two inductors are stacked, the magnetic core of one inductor provides a low reluctance path for the DM magnetic flux of the other one. For example, B_1' and B_4' will flow through the core of the top inductor. This increases the DM (leakage) inductance of each inductor. However, the DM magnetic flux directions of the two inductors are opposite within a core. For example, B_0', B_1', B_4' is opposite to B_2 and B_5 within the top core. Therefore, the mutual

inductance M is negative between the two DM inductances of the two CM inductors.

Fig. 5(b) shows the side view of the DM magnetic flux distribution of each individual inductor. The magnetic flux in front of the inductor is not shown here. The magnetic field generated by the two inductors is superposed in the air and the side view of the stacked inductor is shown in Fig. 5(c). As shown in Fig. 5(b) and (c), after the two inductors are stacked, the magnetic flux

density below and above the stacked inductor is increased. The reason for this is that the magnetic flux of both inductors is counterclockwise above and clockwise below the stacked inductor. On the other hand, in Fig. 5(c), because the two windings above and below the center plane carry the currents with the same magnitude but opposite directions, most of the leakage magnetic flux within the space between two inductors is canceled. On the center plane, the magnetic flux is parallel to the center plane as the magnetic flux in the z direction is canceled and the flux on the xy plane is increased. These result in a very similar magnetic flux distribution to that of the conventional inductor in Fig. 4(b). The CM and DM inductances of the stacked inductors in the first case are, therefore, very close to those of the conventional CM inductor in Fig. 4(a).

The total DM inductance L_{DM} of the stacked inductor in Fig. 5(c) is given by (6). In (6), L_{DM1} is the DM inductance of each DM inductor and M is the mutual inductance between the two DM inductors

$$L_{DM} = 2L_{DM1} - 2M. \tag{6}$$

Fig. 6(a) shows the exploded view of the proposed stacked inductor in the second case. Each inductor has a DM magnetic flux distribution similar to Fig. 4(a) before stacking. Similarly to the stacked inductor in Fig. 5(a), after the two inductors were stacked, the magnetic core of one inductor provides a low reluctance path for the DM magnetic flux of the other inductor. This increases the DM (leakage) inductance of the two inductors. However, differently from the first case, the DM magnetic flux directions of the two inductors are the same within a core. For example, B_0', B_1', and B_4' is in the same direction as B_2 and B_5 within the top core. Therefore, the mutual inductance M is positive between the two DM inductors.

Fig. 6(b) shows the side view of the DM magnetic flux distribution of each individual inductor. The magnetic flux in front of the inductor is not shown here. The magnetic field generated by the two inductors is superposed in the air and the side view of the stacked inductor is given by Fig. 6(c). As shown in Fig. 6(b) and (c), after the two inductors were stacked, the magnetic flux density below and above the stacked inductor is decreased since the magnetic flux of the individual inductors has different directions above and below the stacked inductor. The magnetic flux is perpendicular to the center plane because the magnetic flux on xy plane is canceled and the flux in z direction is increased on the center plane. The DM inductance L_{DM_P} is given by

$$L_{DM\_P} = 2L_{DM1} + 2M = L_{DM} + 4M. \tag{7}$$

In (7), L_{DM_P} is the total DM inductance of the proposed stacked inductor. It is *4M* larger than that of the conventional inductor in Fig. 4(a).

C. Reduced Magnetic Field Emission

It is shown in Figs. 5(c) and 6(c) that the proposed stacked inductor emits a smaller magnetic flux density than the conventional CM inductor in the space above and below the inductors for the reason analyzed previously. The magnetic field generated by CM currents is not discussed here since most of the
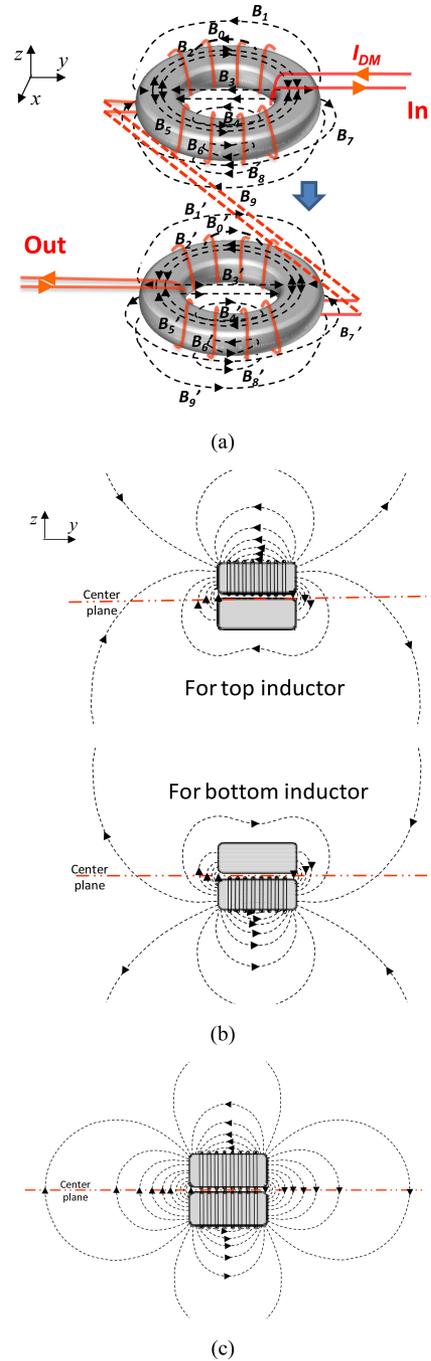

Fig. 6. DM magnetic flux distribution of a stacked inductor with the proposed winding structure: (a) two inductors stacked together with opposite winding directions, (b) DM magnetic flux of two inductors, and (c) side view of the DM magnetic flux distribution of the proposed stacked inductor (the flux in front of the inductor is not shown).

CM magnetic flux is confined within the core due to its high permeability. Fig. 7(a) and (b) shows the simulated DM magnetic flux distributions in Ansys Maxwell 3-D on an xy plane 35 mm above the inductors. In the simulation, the magnetic core has a relative permeability 2000. The outer diameter of the core is 28 mm and the inner diameter of the core is 12 mm. The thickness of a single core is 6.5 mm. The DM current is 100 mA in the simulation. Based on the simulation results, the
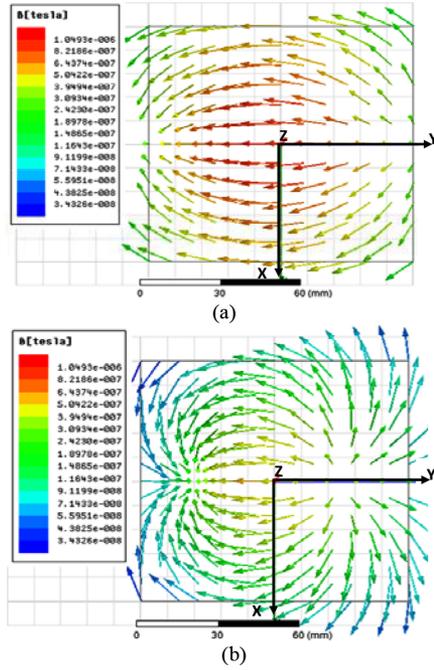
(a)

(b)

Fig. 7. Simulated DM magnetic field distributions on an xy plane 35 mm above the stacked inductors: (a) magnetic field of the conventional CM inductor and (b) magnetic field of the proposed CM inductor.

(a)

(b)

Fig. 8. Simulated DM magnetic field distributions on an xz plane 35 mm away from the stacked inductors: (a) magnetic field of the conventional CM inductor and (b) magnetic field of the proposed CM inductor.

proposed stacked inductor reduces the magnetic flux density by up to 2/3.

For the magnetic flux density on the left and right sides, in the vicinity of the stacked inductor, the proposed stacked inductor increases the flux density. This is because, for the magnetic flux of the individual inductors in Figs. 5(b) and 6(b), the z-component is larger than the x- and y-components in the vicinity of the inductor. However, as distance increases, the proposed stacked inductor emits a smaller magnetic flux density than the conventional one because the z-component becomes smaller than the x- and y-components. Fig. 8(a) and (b) shows the simulated DM magnetic flux distribution on an xz plane, which is 35 mm away from the stacked inductor. Based on the simulation results, the proposed stacked inductor reduces the magnetic flux density by up to 2/3.

The magnetic flux distributions on the front side of the conventional CM inductor with the same winding direction and the proposed stacked inductor are illustrated in Fig. 9(a) and (b), respectively. As previously analyzed, the magnetic flux of the stacked CM inductor with the same winding direction is the same as that of the conventional CM inductor. For the flux in front of the stacked inductor with the same winding direction in Fig. 9(a), the z-component is smaller than the x- and y-components. Therefore, after the flux superposition, the flux density is increased because the x- and y-components of the two inductors add constructively. The flux on the center plane is parallel to the plane because the z-component is canceled out. The dashed lines B_{7A}, B_{7B}, B_{7C}, and B_{7D} represent the magnetic flux flowing on the front side. Half of the flux is above the center plane and half of the flux is below the center plane. The
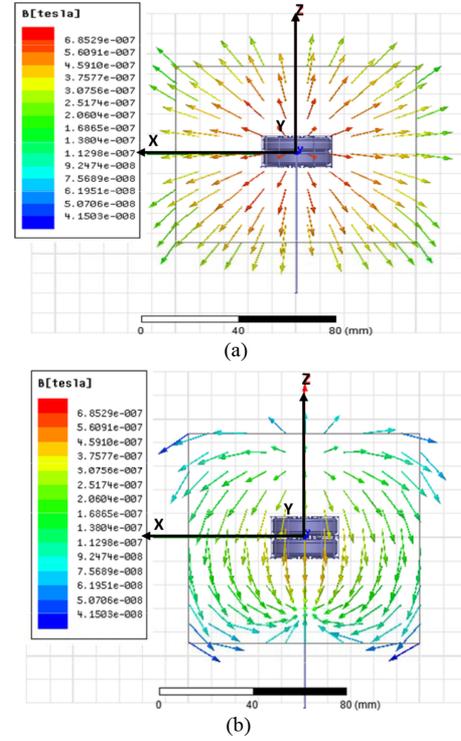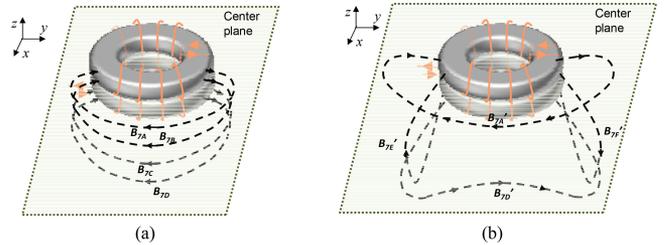

Fig. 9. Comparison of magnetic flux distributions on the front side: (a) stacked CM inductor with the same winding direction and (b) stacked CM inductor with opposite winding directions (proposed).

magnetic flux distribution on the back side is the same as that on the front side and is not shown in the figure.

For the flux of the proposed stacked inductor with opposite winding directions in Fig. 9(b), the scenario is different from that in Fig. 9(a). Similarly to Fig. 6(c), the magnetic flux distribution in the front has four regions: the top, bottom, left, and right regions. In the top region, the flux flows from the right to the left. In the bottom region, the flux flows from the left to the right. In the middle of the top and bottom regions, the z-component is smaller than the x- and y-components and the x- and y-components of one inductor are opposite to those of the other inductor. Therefore, after the flux superposition, the flux density is decreased. The flux is parallel with the center plane in the middle as shown by B'_{7A} and B'_{7D} in Fig. 9(b). Based on the previous analysis, the magnitude of the magnetic flux density of the proposed stacked inductor is smaller
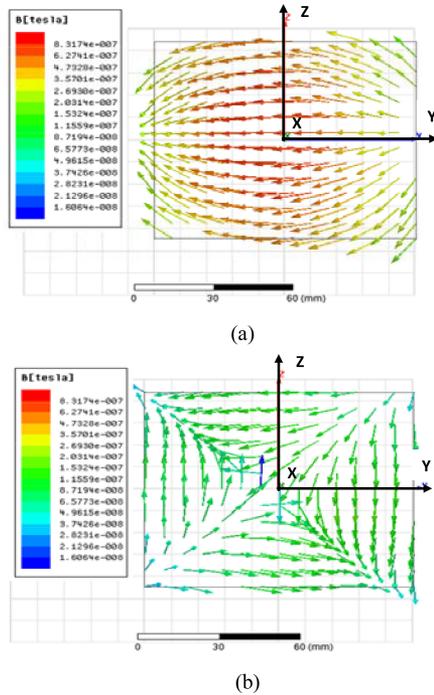
(a)

(b)

Fig. 10. Simulated DM magnetic field distribution on a *yz* plane 22 mm in front of the stacked inductors: (a) DM magnetic field distribution of the conventional CM inductor and (b) DM magnetic field distribution of the proposed CM inductor.
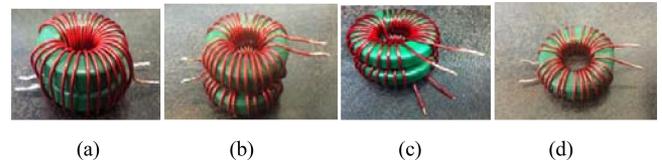

Fig. 11. CM inductor prototypes: (a) CM inductor with two stacked cores, (b) stacked CM inductor with the proposed winding structure, (c) stacked CM inductor with the same winding direction, and (d) CM inductor with only one magnetic core.
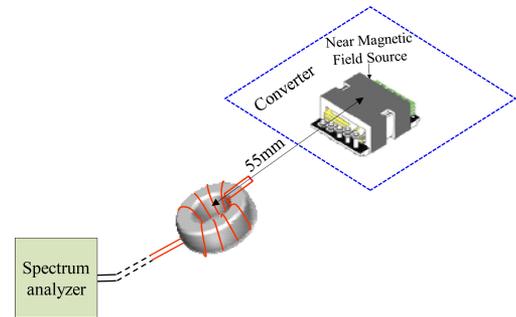

Fig. 12. Measurement setup to test the susceptibility of the CM inductors.

than that of the conventional inductor in the top and bottom regions.

For the left and right regions, the magnetic flux flows from the bottom to the top in the left region and from the top to the bottom in the right region. In the vicinity of the stacked inductor, the proposed stacked inductor increases the flux density because for the magnetic flux of the individual inductors, the *z*-component is larger than the *x*- and *y*-components. However, the proposed stacked inductor has a smaller magnetic flux density than the conventional one as distance increases because the *z*-component becomes smaller than the *x*- and *y*-components. The flux is perpendicular to the center plane because the x and *y*-components are canceled on the center plane as shown by B'_{7E} and B'_{7F} in Fig. 9(b).

Fig. 10(a) and (b) shows the simulated magnetic flux distribution in Ansys Maxwell 3-D on a *yz* plane, which has a distance of 22 mm from the front side of the stacked inductors in Fig. 9(a) and (b). The simulated results show that the proposed stacked inductor reduces the magnetic flux density by up to 2/3. The four magnetic flux regions are clearly shown in Fig. 10(b) for the proposed stacked inductor.

III. EXPERIMENTAL VALIDATION AND DISCUSSION

Four CM inductor prototypes are shown in Fig. 11. The model number of the magnetic cores used in all of these inductors is TN200B H28–16–6.5C from TDG Holding Co., Ltd. The outer diameter and the inner diameter of the core are 28 and 14 mm, respectively. The height of the core is 6.5 mm and its initial relative permeability is 2000. The number of turns for all of

the inductors is 14. The wire used in the inductors is AWG #20. Fig. 11(a) shows a CM inductor with two 14-turn windings wound on two stacked cores. Fig. 11(b) shows a stacked CM inductor with the proposed winding structure. Fig. 11(c) shows a stacked CM inductor with the same winding direction. As discussed in Section II-B, the prototypes in Fig. 11(a) and (c) should have very similar electrical parameters and magnetic field distribution. Fig. 11(d) shows a CM inductor with only one magnetic core.

A. Verification of Near-Field Coupling Suppression

To verify the magnetic field immunity of the proposed CM inductor, susceptibility measurements and comparisons were conducted for the inductors in Fig. 11(a) and (b). These two prototypes were exposed to a near magnetic field generated by a forward converter which has been discussed in [2]. According to [2], the near magnetic field was mainly emitted by the planar transformer of the forward converter. In the experiment, the forward converter had an input/output voltage of 48 V/6 V and an output current of 14 A. The inductor prototypes were 55 mm away from the transformer and located on the exposed winding side of the transformer as shown in Fig. 12.

The windings of the two inductors were connected in parallel to each other to measure the induced CM voltages and in series to measure the induced DM voltages as shown in Fig. 13. Based on the definition of DM voltage, the measured voltages in Fig. 13(b) and (d) were actually twice the value of the actual DM voltages. Therefore, the measured voltages in Fig. 13(b) and (d) were transformed to DM voltages by deducting 6 dB.

The spectra of the induced CM and DM voltages were measured with an Agilent 4395A spectrum analyzer and the measurement results are shown in Fig. 14. In Fig. 14(a) and (b),
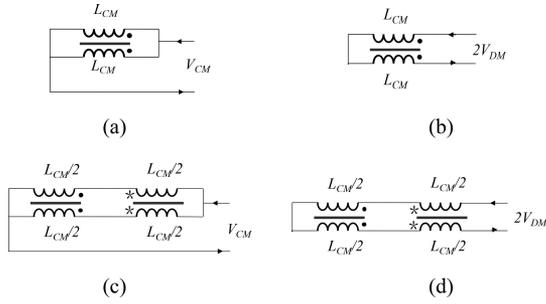
Fig. 13. Setup to measure CM and DM voltages: (a) CM voltage measurement for the conventional CM inductor, (b) DM voltage measurement for the conventional CM inductor, (c) CM voltage measurement for the proposed CM inductor, and (d) DM voltage measurement for the proposed CM inductor.
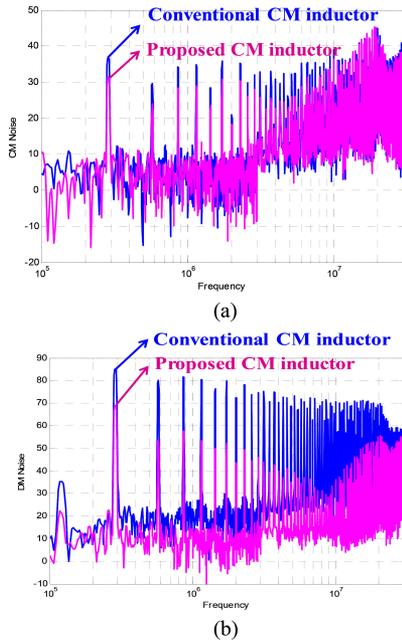

Fig. 14. Comparison of the measured spectra: (a) spectra of the induced CM voltages and (b) spectra of the induced DM voltages.

compared with the conventional CM inductor, the proposed stacked CM inductor reduces both CM noise and DM noise within a wide frequency range by up to 40 dB.

B. Verification of Increased Leakage Inductance

To verify that the proposed CM inductor has an increased leakage inductance, both CM and DM impedances of all inductors in Fig. 11 were measured with an Agilent 4395A impedance analyzer. The configurations for CM and DM impedance measurement are shown in Fig. 15(a) and (b), respectively.

Fig. 16(a) and (b) shows the measured CM and DM impedances for the four CM inductors. As expected, the CM impedances for the first three inductors were almost equal to each other and were twice that of the fourth inductor at low frequency (LF). This is because the LF impedance of a CM inductor is mainly determined by its CM inductance [11], [24]. Based on the LF DM impedances, the proposed stacked CM inductor
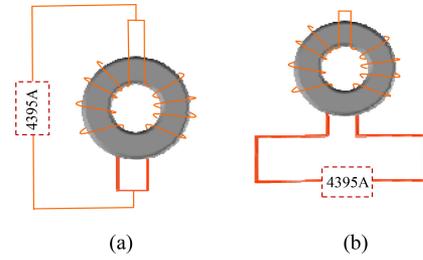

Fig. 15. CM and DM impedance measurement setup: (a) CM impedance measurement configuration and (b) DM impedance measurement configuration.
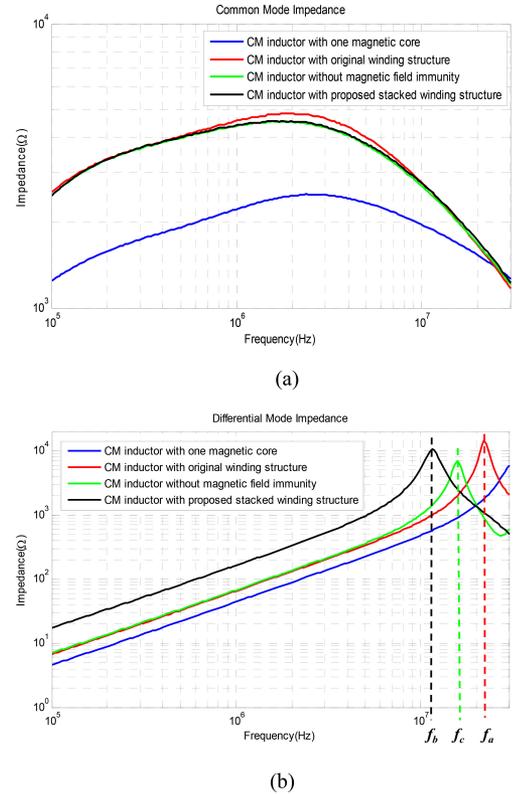

Fig. 16. Comparison of measured impedances for the four CM inductors: (a) CM impedance and (b) DM impedance.

has the highest DM inductance, $L_{\mathrm{DM\_P}}$, of 26 μH. This verifies the analysis in Section II-B. The conventional CM inductor gives a DM inductance of 10.4 μH and the stacked inductor with the same winding directions gives a DM inductance of 11 μH. As predicted in Section II-B, these two inductances are almost equal to each other. Based on (6), (7) and the measured LF DM impedances in Fig. 16(b), L_{DM1} is 9.25 μH and M is 3.75 μH. The inductor with one core only gives a DM inductance of 7 μH. As predicted in Section II-B, the stacked CM inductor increases the self-DM inductance for each inductor from 7 to 9.25 μH. This also verifies the previous analysis.

The equivalent winding capacitance C_P of the DM impedances in Fig. 16(b) can be calculated based on the parallel resonant frequencies in Fig. 16(b) [11]. For the conventional CM inductor in Fig. 11(a), the parallel resonant frequency f_a is

22 MHz, where the impedance peak occurs. C_P can be determined from

$$C_P = \frac{1}{(2\pi f_a)^2 L_{\text{DM}}}. \tag{8}$$

The calculated C_P is 5 pF. The equivalent winding capacitance of the other three DM impedances can be determined similarly. For the proposed stacked inductors in Fig. 11(b) because of the increased parasitic capacitance between the windings on the facing areas of the two inductors, the equivalent winding capacitance increases to 7.5 pF. The parallel resonant frequency reduces to f_b (11.5 MHz) due to the increased DM inductance and winding capacitance. However, the proposed stacked inductor is still preferred because its higher DM inductance delivers better performance at low frequencies, which is important to reduce the size of DM filters [22]. For the stacked inductor with same winding direction in Fig. 11(c), its resonant frequency reduces to f_c (15.7 MHz). Based on (8), its equivalent winding capacitance increases to 9.3 pF. As this structure reduces the DM inductor's high-frequency performance without any advantages at LF, it is not preferred.

C. Verification of Reduced Magnetic Field Emission

To verify that the proposed stacked CM inductor has a reduced magnetic field emission, the measured magnetic fields from the CM inductors shown in Fig. 11(a) and 11(b) were compared. The magnetic fields were measured on a plane 35 mm above the CM inductors. A Rigol DG1022U signal generator, a 10-W RF power amplifier, a Beehive Electronics 100-A EMC probe, a coordinate plane and an Aglient 4395A spectrum analyzer were used in the measurements, as shown in Fig. 17(a).

The inductor prototypes were in the center and under the coordinate board. The coordinate had a dimension of 100 mm × 100 mm with an 11 × 11, 10-mm-spaced grid, as shown in Fig. 17(a). The distance between the inductor and top surface of the coordinate board above the inductor was 35 mm. A 500-kHz sinusoidal voltage signal from the signal generator was amplified by the RF amplifier and fed to the inductor prototypes as a DM current excitation as shown in Fig. 17(b). The amplitude of the 500-kHz voltage signal was adjusted until the amplitude of the DM current reached 100 mA. The EMC probe was connected to the spectrum analyzer in order to read the amplitude of the EMC probe's output voltage. The DM magnetic field generated by the inductor under the coordinate board was measured point by point by changing the locations and directions of the EMC probe on the coordinate board. The magnetic flux densities were measured at each point on the 11 × 11, 10-mm-spaced grid (a total 121 points) in Fig 17(a). For each point, the EMC probe was placed in the *x*-, *y*-, and *z*-directions as shown in Fig. 17(a). The measured data in the *x*-, *y*-, and *z*-directions at 500 kHz were converted to B_x, B_y, and B_z, respectively, based on the manufacturer's formula. Finally, the magnitude of the magnetic flux density at each point can be calculated based on
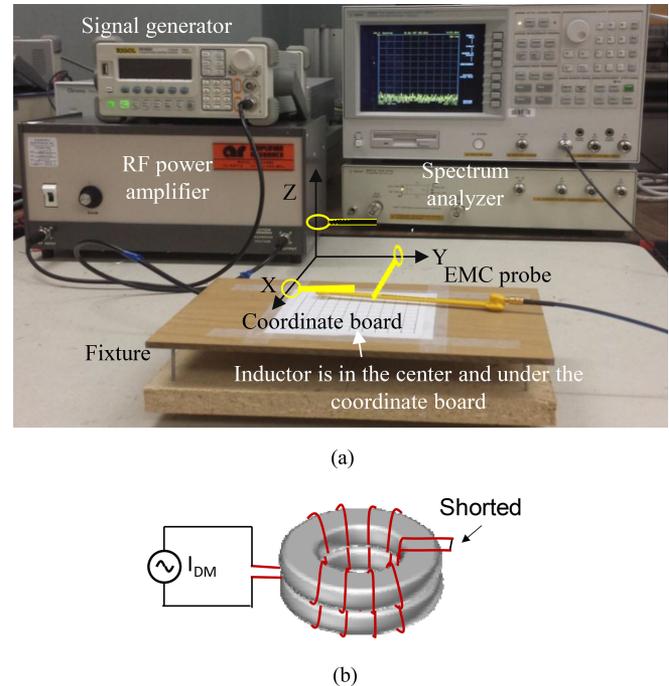
$$B = \sqrt{B_x^2 + B_y^2 + B_z^2}. \tag{9}$$

Fig. 17. Test setup to measure the magnetic field distribution of inductor prototypes: (a) measurement setup and (b) DM current excitation added to an inductor prototype.

The final magnetic flux densities of the CM inductor in Fig. 11(a) and (b) are shown in Fig. 18(a) and (b), respectively. It is shown in Fig. 18(a) and (b) that the proposed stacked CM inductor reduces the emitted magnetic flux density by up to 2/3, as predicted by the simulation.

D. Conducted EMI Measurement

In Fig. 19(a), the in-circuit performance of the CM inductors in Fig. 11(a) and (b) was tested with the same forward converter and load conditions as those in Fig. 12. The CM inductor prototypes were also placed at the same position as those in Fig. 12. The CM inductors in Fig. 11(a) and (b) were used as the CM inductor of an L-type EMI filter between the dc source and the converter. Line impedance stabilization networks and a noise separator [23] are used to measure the conducted CM and DM noise of the forward converter as shown in Fig. 19.

The EMI filter has both DM and CM capacitors as shown in Fig. 19. The measured CM and DM noise spectra of the forward converter with the two inductor prototypes are shown in Fig. 20. As shown in Fig. 20(a), the proposed stacked CM inductor can reduces CM noise by up to 6 dB because of the reduced near-magnetic-field coupling. As shown in Fig. 20(b), the proposed stacked CM inductor greatly reduces DM noise (by up to 40 dB) due to the reduced near magnetic-field-coupling and the increased DM inductance. It should be noted that the spectra in Fig. 20 agree with those in Fig. 14. This indicates that the near-magnetic-field coupling contributes most of the measured EMI noise. Under this condition, increasing the DM/CM capacitance or the DM/CM inductance in the original circuit will not efficiently reduce EMI noise.
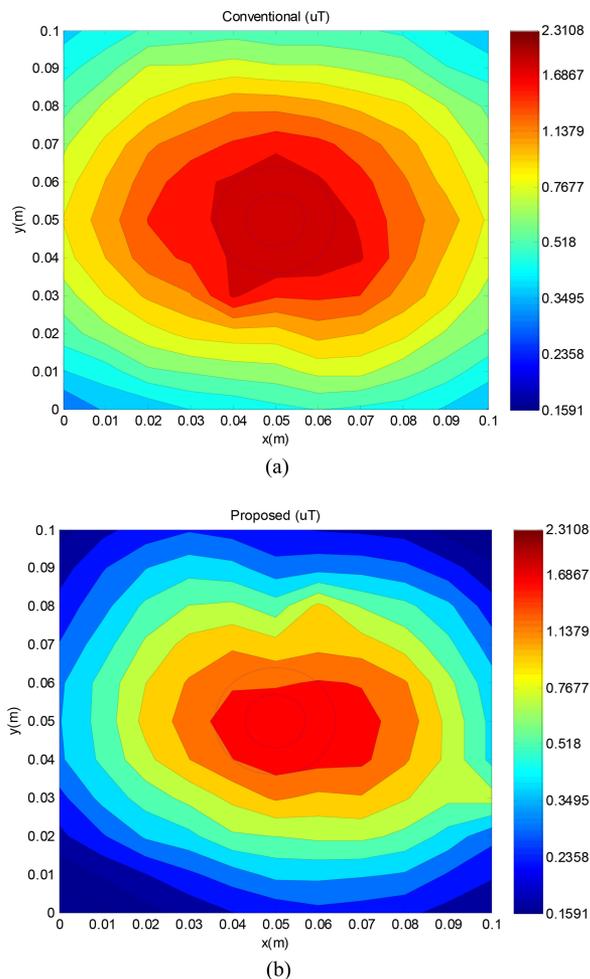
(a)

(b)

Fig. 18.   Measured magnetic field emitted by the inductors due to DM current excitations for: (a) conventional CM inductor and (b) proposed stacked CM inductor.

As shown in Fig. 20, the CM noise is below the EMI standard EN55022, but the DM noise is above the standard. To attenuate the DM noise, a DM capacitor was added between the dc source and the CM inductor prototypes. With the proposed stacked CM inductor, a 2.2-μF DM capacitor was enough to reduce the total noise to below the standard as shown in Fig. 21. On the other hand, with the conventional CM inductor, an 82-μF DM capacitor was needed to reduce the total noise to below the standard as shown in Fig. 22. The proposed staked CM inductor can, therefore, reduce the size of the DM capacitor, as well as the total volume of the EMI filter.

E. Discussion

As discussed previously, the proposed stacked CM inductor demonstrates three advantages over the conventional CM inductor as discussed previously. First, it has external magnetic field immunity. In the experiments above, the induced DM noise was reduced by up to 40 dB (a factor of 100) by replacing the conventional CM inductor with the proposed stacked inductor. Second, it has an increased DM inductance. In the experiments

(a)

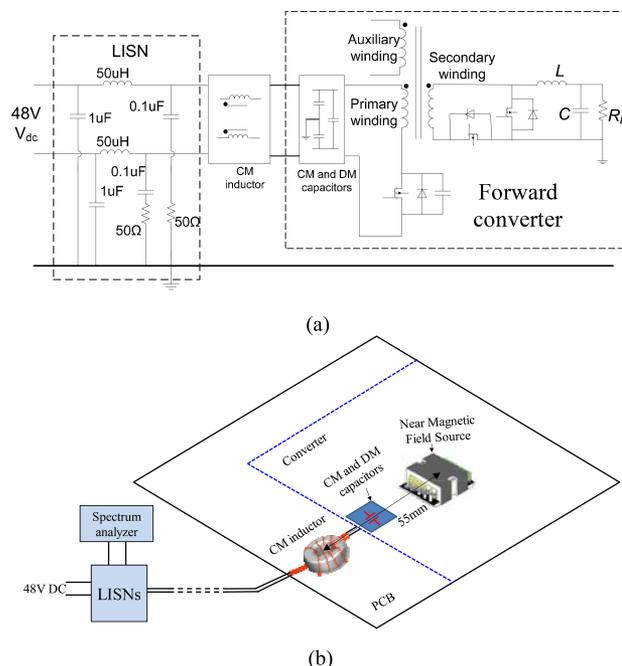(b)

Fig. 19.   (a) Topology of the forward converter and (b) measurement setup.
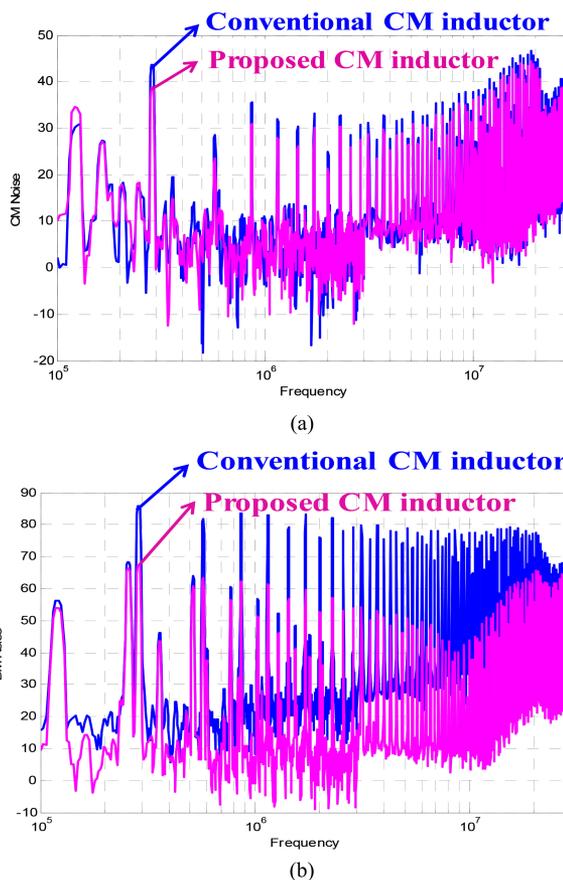

(a)

(b)

Fig. 20.   Comparison of the measured EMI noise with the conventional CM inductor and the proposed stacked CM inductor: (a) CM noise and (b) DM noise.
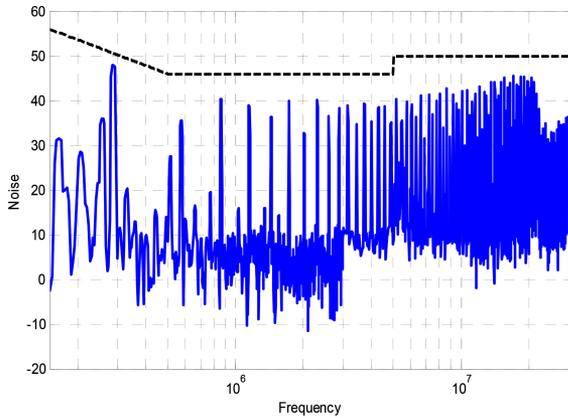
Fig. 21. Total noise of the forward converter with the proposed CM inductor and an extra 2.2-μF DM capacitor.
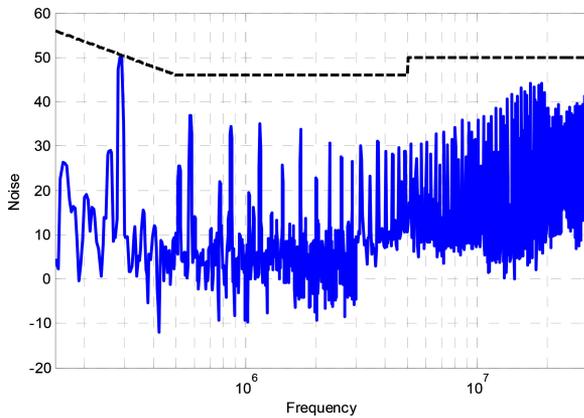

Fig. 22. Total noise of the forward converter with the conventional CM inductor and an extra 82-μF DM capacitor.

Fig. 23. Size comparison of a 2.2 and an 82-μF/100 V electrolytic capacitors.

above, the DM inductance was increased by 136% from that of the conventional CM inductor. Furthermore, the stacked CM inductor emits a much lower magnetic flux density than the conventional CM inductor. In the experiments, the emitted near magnetic flux density was reduced by 2/3.

On the other hand, the inductor volume and the winding resistance are slightly increased. The cost of the CM inductor may also be slightly increased. However, the total volume and the total cost of the EMI filter components may be reduced because a significantly smaller DM capacitor can be used with the proposed stacked CM inductor. Fig. 23 shows the size comparison of a 2.2 μF and an 82-μF DM electrolytic capacitor.

The calculation shows that the volume of the CM inductor is increased by 1 cm^3 due to two more layers of winding on the proposed stacked CM inductor. However, the volume of the DM capacitor is reduced by 2.26 cm^3, so the total volume of the EMI filter components is actually reduced by 1.26 cm^3. Furthermore, the footprint of the EMI filter is also reduced by 0.59 cm^2 with the proposed stacked CM inductor due to the size reduction of the DM capacitor.

As for the increased winding resistance, the calculated power loss is increased by only 0.032 W, which is negligible for an 84-W converter. Therefore, the extra winding resistance will not cause any problems except in very high-current applications.

Although the cost of the CM inductor is increased, the cost of the DM capacitor is reduced, so the total cost would not change much.

Based on the discussion aforesaid, replacing the conventional single core CM inductor with the proposed stacked CM inductor offers significant benefits.

IV. CONCLUSION

This paper proposes a novel stacked CM inductor with improved electromagnetic performance. The stacked CM inductor is composed of two CM inductors that have identical cores and the same number of winding turns but with opposite winding directions. The induced noise voltages due to near-magnetic-field coupling within these two inductors cancel each other. The proposed stacked CM inductor also has a higher DM inductance than conventional CM inductors. The increased DM inductance helps to reduce DM noise. Furthermore, the proposed stacked CM inductor has a lower DM near-magnetic-field emission than conventional CM inductors, so the proposed technique also reduces the near-magnetic-field interference due to the DM currents in CM inductors. Both simulation and experimental results verify the advantages of the proposed stacked CM inductor over conventional CM inductors.

REFERENCES

[1] R. Wang, H. F. Blanchette, M. Mu, and D. Boroyevich, "Influence of high-frequency near-field coupling between magnetic components on EMI filter design," *IEEE Trans. Power Electron.*, vol. 28, no. 10, pp. 4568–4579, Oct. 2013.

[2] Y. Chu, S. Wang, J. Xu, and D. Fu, "EMI reduction with near field coupling suppression techniques for planar transformers and CM chokes in switching-mode power converters," in *Proc. IEEE Energy Convers. Congr. Expo.*, 2013, pp. 3679–3686.

[3] R. Lai, Y. Maillet, F. Wang; S. Wang, R. Burgos, and D. Boroyevich, "An integrated EMI inductor for differential-mode and common-mode noise suppression," *IEEE Trans. Power Electron.*, vol. 25, no. 3, pp. 539–544, Mar. 2010.

[4] W. Tan, C. Cuellar, X. Margueron, and N. Idir, "A Common-mode choke using toroid-EQ mixed structure," *IEEE Trans. Power Electron.*, vol. 28, no. 1, pp. 31–35, Jan. 2013.

[5] L. Nan and Y. Yugang, "A common mode and differential mode integrated EMI filter," in *Proc. IEEE Trans. Power Electron. Motion Control Conf.*, Aug. 14–16, 2006, vol. 1, pp. 1–5.

[6] I. F. Kovacevic, T. Friedli, A. M. Muesing, and J. W. Kolar, "3-D electromagnetic modeling of EMI input filters," *IEEE Trans. Ind. Electron.*, vol. 61, no. 1, pp. 231–242, Jan. 2014.

[7] I. F. Kovacevic, T. Friedli, A. M. Muesing, and J. W. Kolar, "3-D electromagnetic modeling of parasitics and mutual coupling in EMI filters," *IEEE Trans. Power Electron.*, vol. 29, no. 1, pp. 135–149, Jan. 2014.

[8] T. Q. V. Hoang, A. Breard, and C. Vollaire, "Near magnetic field coupling prediction using equivalent spherical harmonic sources," *IEEE Trans. Electromagn. Compat.*, vol. 56, no. 6, pp. 1457–1465, Dec. 2014.

[9] S. Wang, F. C. Lee, D. Y. Chen, and W. G. Odendaal, "Effects of parasitic parameters on EMI filter performance," *IEEE Trans. Power Electron.*, vol. 19, no. 3, pp. 869–877, May 2004.

[10] S. Wang, F. C. Lee, W. G. Odendaal, and J. D. Van Wyk, "Improvement of EMI filter performance with parasitic coupling cancellation," *IEEE Trans. Power Electron.*, vol. 20, no. 5, pp. 1221–1228, Sep. 2005.

[11] S. Wang, F. C. Lee, and J. D. Van Wyk, "Design of inductor winding capacitance cancellation for EMI suppression," *IEEE Trans. Power Electron.*, vol. 21, no. 6, pp. 1825–1832, Nov. 2006.

[12] L. Taylor, W. Tan, X. Margueron, and N. Idir, "Reducing of parasitic inductive couplings effects in EMI filters," in *Proc. IEEE 15th Power Electron. Appl. Conf.*, 2013, pp. 1–8.

[13] G. Asmanis, A. Asmanis, and D. Stepins, "Mutual couplings in three phase T-type EMI filters," in *Proc. IEEE Int. Symp. Electromagn. Compat.*, 2012, pp. 1–6.

[14] J. He, W. Chen, and J. Jiang, "Identification and improvement of stray coupling effect in an L-C-L common mode EMI filter," in *Proc. CES/IEEE Int. Power Electron. Motion Control Conf.*, 2006, pp. 1–5.

[15] C. Labarre, F. Costa, and J. Ecrabey, "Correlation between the near magnetic field radiated by an EMI filter and its electric working," in *Proc. IEEE Vehicle Power Propulsion Conf.*, 2010, pp. 1–5.

[16] H. Chen and Z. Qian, "Modeling and characterization of parasitic inductive coupling effects on differential-mode EMI performance of a boost converter," *IEEE Trans. Electromagn. Compat.*, vol. 53, no. 4, pp. 1072–1080, Nov. 2011.

[17] C. Labarre and F. Costa, "Circuit analysis of an EMI filter for the prediction of its magnetic near-field emissions," *IEEE Trans. Electromagn. Compat.*, vol. 54, no. 2, pp. 290–298, Apr. 2011.

[18] J. He, J. Jiang, and W. Chen, "Identification and model of near field magnetic coupling in a PFC converter," in *Proc. IEEE Power Electron. Spec. Conf.*, pp. 323–327.

[19] L. Feng, W. Chen, H. Chen, and Z. Qian, "Study on the conducted EMI due to radiated coupling in SMPS," in *Proc. IEEE Appl. Power Electron. Conf.*, 2006, pp. 1161–1164.

[20] K. Mainali and R. Oruganti, "Conducted EMI mitigation techniques for switch-mode power converters: A survey," *IEEE Trans. Power Electron.*, vol. 25, no. 9, pp. 2344–2356, Sep. 2010.

[21] F. Luo, D. Dong, D. Boroyevich, P. Mattavelli, and S. Wang, "Improving high-frequency performance of an input common mode EMI filter using an impedance-mismatching filter," *IEEE Trans. Power Electron.*, vol. 29, no. 10, pp. 5111–5115, Oct. 2014.

[22] S. Fu-Yuan, Y.-T. Chen, Y.-P. Wu, and Y.-T. Chen, "A procedure for designing EMI filters for AC line applications," *IEEE Trans. Power Electron.*, vol. 11, no. 1, pp. 170–181, Jan. 1996.

[23] S. Wang, Fred C. Lee, and W. G. Odendaal, "Characterization, evaluation and design of noise separator for conducted EMI noise diagnosis," *IEEE Trans. Power Electron.*, vol. 20, no. 4, pp. 974–982, Jul. 2005.

[24] S. Wang, Fred C. Lee, and W. G. Odendaal, "Single layer iron powder core inductor model and its effect on boost PFC EMI noise," in *Proc. Power Electron. Spec. Conf.*, Jun. 15–19, 2003, pp. 847–852.

Shuo Wang (S'03–M'06–SM'07) received the Ph.D. degree from Virginia Tech, Blacksburg, VA, USA, in 2005.

He has been with the Department of Electrical and Computer Engineering, University of Florida, Gainesville, FL, USA, since 2015. From 2010 to 2014, he was with University of Texas at San Antonio, TX, USA, first as an Assistant Professor and later as an Associate Professor. From 2009 to 2010, he was a Senior Design Engineer in GE Aviation Systems, Vandalia, OH, USA. From 2005 to 2009, he was a Research Assistant Professor at Virginia Tech.

Dr. Wang has published more than 100 IEEE journal and conference papers and holds seven US patents. He received the Best Transaction Paper Award from the IEEE Power Electronics Society in 2006 and two William M. Portnoy Awards for the papers published in the IEEE Industry Applications Society in 2004 and 2012, respectively. In 2012, he received the prestigious National Science Foundation Career Award. He is an Associate Editor for the IEEE TRANSACTIONS ON INDUSTRY APPLICATIONS and a technical program Co-Chair for IEEE 2014 International Electric Vehicle Conference.

Ning Zhang received the Bachelor and Master degrees from Xiangtan University and University of Texas at San Antonio in 2008 and 2014, respectively. He has been with TOSHIBA International Corporation, Houston, TX, USA, since 2014.

He has authored and coauthored several IEEE conference and Transaction papers.

Dianbo Fu (M'09) received the B.S. degree from Huazhong University of Science and Technology, Wuhan, China, and the M.S. and Ph.D. degrees from Virginia Polytechnic Institute and State University, respectively.

In 2010, he joined Huawei Technologies, Plano, TX, USA, where he has been engaged in product design, research and development. His interests include high-frequency power conversion, soft-switching techniques, magnetic design, electromagnetic interference, telecom power conversion, and power inversion techniques.

Dr. Fu holds two U.S. patents, and has six U.S. patents pending. He also received the William M. Portnoy Award from the IEEE Industry Applications Society in 2012.

Yongbin Chu (S'12) received the B.S.E.E degree from Hefei University of Technology, Hefei, China, in 2011. He is currently working toward the Ph.D. degree from the University of Texas at San Antonio, TX, USA.

His research interest includes circuit topology for power electronics, electromagnetic interference/electromagnetic compatibility in power electronics systems, high-efficiency and high power density power conversion, and power systems analysis.